Pavement distress detection and avoidance for intelligent vehicles

Mauro Bellone*

Chalmers University of Technology,
41296, Göteborg, Sweden
Email: mauro.bellone@chalmers.se
*Corresponding author

Giulio Reina

Department of Engineering for Innovation,
Universitá del Salento,
Via Arnesano, 73100 Lecce, Italy
Email: giulio.reina@unisalento.it

Abstract: Pavement distresses and potholes represent road hazards that can cause accidents and damages to vehicles. The latter may vary from a simple flat tyre to serious failures of the suspension system, and in extreme cases to collisions with third-party vehicles and even endanger passengers' lives. The primary scientific aim of this study is to investigate the problem of road hazard detection for driving assistance purposes, towards the final goal of implementing such a technology on future intelligent vehicles. The proposed approach uses a depth sensor to generate an environment representation in terms of 3D point cloud that is then processed by a normal vector-based analysis and presented to the driver in the form of a traversability grid. Even small irregularities of the road surface can be successfully detected. This information can be used either to implement driver warning systems or to generate, using a cost-to-go planning method, optimal trajectories towards safe regions of the carriageway. The effectiveness of this approach is demonstrated on real road data acquired during an experimental campaign. Normal analysis and path generation are performed in post-analysis. This approach has been demonstrated to be promising and may help to drastically reduce fatal traffic casualties, as a high percentage of road accidents are related to pavement distress.

Keywords: intelligent vehicles; pavement distress detection; advanced driving assistance systems; road analysis; 3D point cloud.

Reference to this paper should be made as follows: Bellone, M. and Reina, G. (2016) 'Pavement distress detection and avoidance for intelligent vehicles', *Int. J. Vehicle Autonomous Systems*, Vol. 13, No. 2, pp.152–167.

Biographical notes: Mauro Bellone received the MS degree in Automation Engineering from the University of Salento, Italy, where he received the PhD in Mechanical and Industrial Engineering in 2014. In 2013–2014, as visiting researcher at University of Almería, Spain, he has worked with the Automatic, Electronic and Robotics Research Group studying new advanced navigation techniques for mobile robotics and autonomous driving. At the present, he is a

post-doc researcher in the adaptive systems research group of Chalmers University of Technology in Sweden, where he is currently conducting researches on autonomous driving systems for trucks.

Giulio Reina received the Laurea degree and the Research Doctorate degree from the Politecnico of Bari, Italy, in 2000 and 2004, respectively, both in Mechanical Engineering. From 2002 to 2003, he worked at the University of Michigan Mobile Robotics Laboratory as a Visiting Scholar. In 2007, he was awarded a Japanese Society for Promotion of Science fellowship for a 1-year research at the Space Robotics Laboratory of the Tohoku University, Sendai, Japan. In 2010, he was also selected to receive an Endeavour Research Fellowship at the Australian Centre for Field Robotics of the University of Sydney, Australia. Currently, he is an Assistant Professor in Applied Mechanics with the Department of Engineering for Innovation, University of Salento, Lecce, Italy. His research interests include mobile robotics for planetary exploration, vehicle dynamics, and advanced driving assistance systems for automotive and agriculture.

1 Introduction

From a report of the Italian Institute for Statistics (ISTAT, 2013) a total of 1528 road accidents were caused by pavement distresses and road irregularities in 2012. In particular, 893 of the total accidents occurred on urban roads and 635 on highways. At the same time, on the other side of the world, 1051 pothole-related accidents occurred in Korea (Kim and Ryu, 2014), and among 4223 pothole-related accidents between 2008 and 2013 up to 2961 accidents happened on regional highways, which is 70.1% of total pothole accidents. Furthermore, the American Society of Civil Engineers recently studied the effects of pavement surface conditions on traffic crash severity (Lee et al., 2015). The results from this study suggest that the severity levels of most of crash types increase in the case of badly maintained pavements. Beside the importance of road maintenance that can be considered as a passive form of safety, the present study proposes the use of 3D cameras as active safety devices to prevent road accidents by detection and avoidance of pavement distresses.

Following such objectives, researchers are working on improving more and more the safety of future vehicles and their global performance; as a consequence, the problem of detecting road surface conditions may provide additional information for controlling vehicles' speed and steering or developing driver warning systems. A past research in this field has used elevation maps for detecting and classifying road surface, such as in Oniga and Nedevschi (2010). A common solution for terrain traversability analysis foresees the definition of a digital elevation map and assigning two indexes to each of its cells: the roughness and the inclination index (Howard and Saraji, 2001; Osari, 2003; Seraji, 1999). The former is defined as the variance of the elevation values in a specific region of the environment, whereas the latter can be obtained as the average angle of adjacent elevation values with respect to their neighbours (Rohmer et al., 2010). As the problem of understanding the road irregularities is under investigation by researchers owing to its practical implication for autonomous vehicles, Broggi et al. (2013) propose a similar approach to detect road irregularities. In such approach, the point cloud is

first smartly sampled into a 2 – 1/2 dimension grid map, then samples are fitted into a rational B-Spline surface by means of re-weighted least square fitting and equalisation. A past approach using Kinect sensor can be found in Joubert et al. (2011), in which the authors propose a method to tag potholes using a plane segmentation based on the point elevation.

As an improvement to these approaches, Bellone et al. (2013a, 2014a) address the problem using the Principal Component Analysis (PCA) and normal vectors analysis, proposing a new point descriptor that includes information of roughness and surface inclination with respect to the camera reference frame. Such descriptor was called Unevenness Point Descriptor (UPD) and it allows the underlying geometric pattern, associated with each single 3D point, to be fully captured, and difficult scenarios including ramps, edges, and negative obstacles to be correctly handled. The UPD was demonstrated in off-road and indoor environments. In this work, it is instead applied in the context of surface analysis in urban challenging roads. Past works on fast 3D normal estimation (Holzer et al., 2011, 2012), in which the authors present efficient methods for the real-time perception and scene segmentation for household environments using normal vectors, have inspired the idea of using a point descriptor to analyse road surface irregularities. The next step after detection and location is pavement distress avoidance, which represents one of the novel contributions of this paper. Hence, this work focuses on the detection of road irregularities and the implementation of a cost function which can be simply used for path planning purposes. The solver used in this application is the Dijkstra's algorithm, yet the generality of the UPD makes it suitable in any other solver as well. The results demonstrate the validity of this system since: (i) it generates safe and free-collision paths in case of uneven pavement; (ii) it can directly work on a 3D-based space reconstruction avoiding DEM processing; (iii) even though no robot geometric shape has been considered, the UPD-based traversability index allows the planner to generate feasible paths thanks to the pre-sizing of a specific parameter for the calculation of the UPD.

The remainder of the paper is organised as follows: Section 2 introduces our custom-built test bed including hardware design and software architecture. Next, Section 3 summarises the concept of traversability estimation using normal vectors and UPD analysis. Then, the concept of UPD is extended to build a cost function for the path planner. Experimental results are presented in Section 4. Finally, the conclusions are drawn in Section 5.

2 System overview

As the high complexity of autonomous systems requires the harmonious combination of hardware and software implementation, following the hardware characteristics of our test bed and the software implementation of the acquisition/elaboration architecture will be thoroughly described.

2.1 Hardware features

For the testing of the system during its development, it was integrated into a commercial car, serving as the experimental test bed, as shown in Figure 1. A Kinect sensor was mounted at the front of the vehicle using a custom-built holder made of aluminium

profiles that ensure lightness and minimal invasiveness. A suction pad is adopted to attach the holder to the car's hood. The holder design and its position were chosen to provide short-range sensing and, at the same time, to optimise the look-ahead distance L_w, as shown in Figure 1(b). In this way, we obtain a longitudinal field of view of about 2 m from the vehicle bumper, considering the vertical view angle of the camera $\alpha = 43$ deg and the sensor inclination angle $\beta = 34$ deg. The holder weights about 1.5 kg. Considering also the weight of the sensor, around 1.3 kg, the two parts assembled have a weight equal to 2.8 kg that is a way less than the suction pad maximum weight capability.

Figure 1 The experimental test bed: (a) A Microsoft Kinect camera was mounted on the front of the test bed; (b) The system design, where α denotes the view angle, β labels the sensor inclination angle, and L_w is the look-ahead distance. In the inset the kinematic chain of the holder of the camera

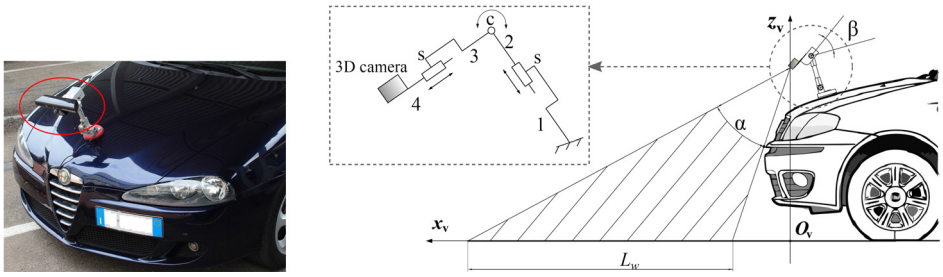

(a) (b)

The holder and its position were conceived considering the specific vehicle and the sensor size. Moreover, it was properly designed to acquire short-range images. The longitudinal field of view ranges from 0.20 m starting from the vehicle bumper, perfectly acceptable for this applications. The maximum distance of about 3.50 m has been properly designed to maximise the capability of the Kinect sensor. However, higher distance should be taken into account for practical applications in order to have enough time for a safe manoeuvre using high-end sensors. As a consequence, our system has been tested only at relatively low-speed.

Figure 1 shows the design of the holder and its assembling scheme on the vehicle. Specifically, the inset in Figure 1(b) shows the kinematic chain of the holder consisting of a two-link mechanism with adjustable length of both arms. The numbers 2 and 3 denote the prismatic joints, whereas the letter 'c' denotes the revolute joint. The number 1 denotes the base joint where the holder is linked to the vehicle. The so-designed structure has three degrees of freedom and it can be simply regulated on different test vehicles. The revolute joint is positioned on the elbow, whereas the sensor is in fixed wrist 4. Figure 1(b) shows the design scheme of the holder assembled on the vehicle showing all fundamental measurements in the vehicle reference frame.

The Kinect camera provides 640×480 RGB-D images at 30 Hz. The sensor comprises a RGB camera and a 3D depth sensor. The RGB video camera provides 8-bit RGB images with resolution of 640×480 pixels. The sensor beam is 57×43 degrees in

horizontal and vertical direction, respectively. The 3D depth sensor consists of an infrared laser emitter and a monochrome depth camera. These two sensors provide a light coding able to acquire information about the distances between the sensor and each pixel in the image. The choice of such sensors has been determined by its cost-effectiveness in comparison with its performance. However, it is well known in the literature that this sensor performs poorly under direct sunlight. Further details on this prototype including camera calibration procedure can be found in Bellone et al. (2014b).

2.2 Software architecture

Processing of the sensor raw data is performed using the Point Cloud Library (PCL) (Rusu and Cousins, 2011). PCL presents an advanced and extensive approach to the subject of 3D perception, providing support for all the common 3D building blocks that applications require. The library contains state-of-the-art algorithms for: filtering, feature estimation, surface reconstruction, registration, model fitting and segmentation. The implemented algorithm includes a filtering stage with statistical outliers removal and voxelisation in order to increase the robustness of our framework. The complete acquisition and analysis framework is shown in Figure 2. It consists of two different stages. The former is the data acquisition framework including camera image capture and RGB-D point cloud reconstruction, this stage includes also filtering and downsampling for efficient data processing; whereas the later consists of a post-elaboration with normal vector estimation and surface interpretation using the UPD. Our application automatically performs filtering to remove outliers and voxelisation. Then the cloud is transformed from the camera reference frame into the vehicle reference and finally saved as a binary file. The post-elaboration iteratively loads point cloud files from memory and estimate normals. Since the UPD needs a search in a neighbourhood during its calculation, our implementation uses KdTree for fast neighbours selection taking a significant part of the computational burden since it needs to be run for every point of the cloud. Performance analysis of UPD including execution time can be found on previous researches (Bellone et al., 2013a,b).

The interpreted 3D point cloud is then divided into a grid of terrain patches of 0.075×0.075 m and projected onto a horizontal plane in order to reconstruct a grid i.e. the traversability map. Each 3D point is mapped to a specific cell of the reference grid. By assessing the unevenness associated with the set of points in each cell, it is possible to assign them a traversability index. Finally the path generation module works on the traversability map computing the path according to possible pavement distresses.

Although data acquisition and elaboration are now performed as separated steps, they could be implemented as a unique application. However, the acquisition frame rate depends on sensor capability, whereas the UPD analysis depends on number of points in the cloud. Past evaluations on UPD calculation performance confirmed the capability to analyse images at 1 Hz on low-performance computers. However, the computational time also depends on the number of neighbours in which the UPD is computed.

Figure 2 The acquisition and interpretation stage features depth camera image acquisition, RGB-D image reconstruction and interpretation via UPD analysis, whereas the path planning stage includes the traversability grid reconstruction and path generation

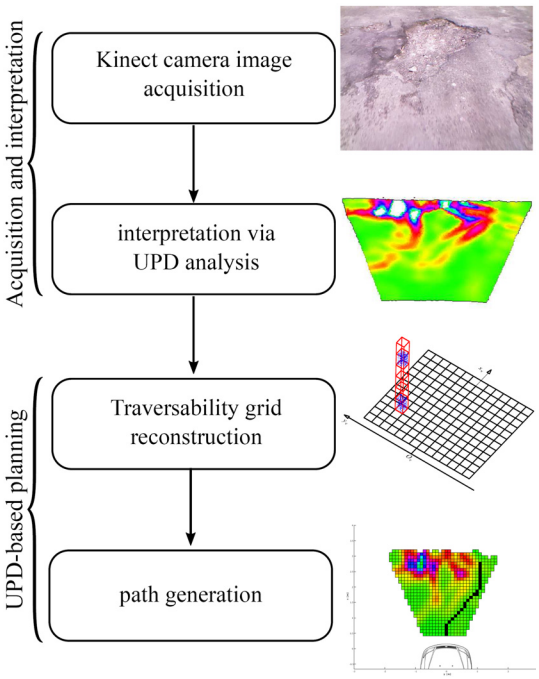

3 Pavement distresses detection and avoidance

This work relies on UPD-based surface analysis for the extraction of local information from a point cloud. In order to provide the necessary background for those unfamiliar with the topic, this section recalls the concept of road surface analysis using the UPD local descriptor. Next, the concept is extended to derivate a cost function for path planning purposes.

3.1 UPD traversability analysis

Perception in urban scenarios requires accurate surface analysis and even though simple and widely used, the point elevation may be not enough for a reliable estimation of terrain traversability. As an alternative solution, we propose the use of normal vectors to estimate surface irregularities. UPD provides an efficient and simple choice to extract traversability information from 3D data. Using PCA and normal analysis for perception (Rusu, 2009; Rusu et al., 2008), the UPD describes surfaces through a normal vectors-based analysis in a ring neighbourhood, resulting in a simple and efficient description of irregularities and inclination.

Summarising the concept, let us consider $P = \left\{ p_i(x_i, y_i, z_i) \in \mathbb{R}^3 \right\}$ as a set of points constituting a point cloud. Then, let us select a query point $p_q \in P$ and consider its neighbourhood defined as follows:

$$P_q^k = \left\{ p_q \in P : | p_i - p_q | \leq d_m \right\}, \tag{1}$$

where, P_q^k is the neighbourhood of the query point p_q with radius d_m which is a scalar value representing the size of the neighbourhood. Now, let us consider $\vec{n}_i$ as the normal vectors computed using the PCA in P_q^k, with $i = 1,2,\ldots,k$, where k is the number of neighbours in P_q^k. Given the above, we can define the *r*-vector as vector sum of the normal vectors in P_q^k, and computed as:

$$\vec{r}_k^q = \sum_{i=1}^{k} \vec{n}_i. \tag{2}$$

One should note that, even though the vector sum is calculated in P_p^k, see equation (1), it includes also the information about the normal vectors of the points located in its vicinity but positioned outside the neighbourhoods. This means that the UPD includes a piece of information not only about the points located inside the neighbourhood, but also about those, which are located in its vicinity. Finally, the UPD in p_q, can be defined as:

$$F_U\left(p_q, P_1^k\right) = \left\{ r_x^q, r_y^q, r_z^q, \zeta_k^q \right\}, \tag{3}$$

where r_x^q, r_y^q and r_z^q are the scalar components of $\vec{r}_k^q$, and ζ_k^q is defined by the following equation (4). The components of $\vec{r}_k^q$ provide information about the global direction of the local surface in the sensor reference frame. On the other hand, the parameter ζ_k^q can be interpreted as a local inverse "unevenness index", since it assesses the degree of local roughness. It depends on the distribution of the direction of the normal vectors in the neighbourhood and it is given by:

$$\zeta_k^q = \frac{\left| \vec{r}_k^q \right|}{k}, \tag{4}$$

where $\vec{r}_k^q$ has been defined in equation (2), and k is the number of neighbours of p_q in P_k^q. By dividing by k, ζ_k^q is normalised and neighbourhoods, including a different number of points, can be compared to each other.

In summary, equation (3) defines a powerful local descriptor that can be used for road/terrain analysis and enhance the traversability awareness of a vehicle. From a mathematical point of view, vertical and horizontal surfaces might be represented by the same value of the unevenness index, since it provides regularity information only, regardless of the surface inclination. Although the horizontal surface can be traversed, the vertical one typically describes obstacles. In Figure 3(a), an explicative example is shown. Here, the ground reference frame is marked as blue arrows and a typical vector belonging to the ground is marked as a green arrow. One should note that a typical

ground normal vector should be aligned with the z-axis. In Figure 3(a), the red arrows mark vectors belonging to objects that may be interpreted as regular surface yet they are not traversable due to their orientation. As the matter of fact, their orientations are typically misaligned with respect to z-axis. Hence, given the query point p_q and its r-vector, the angle α_q between the z-axis and the r-vector can be obtained as:

$$\alpha_q = \arccos\left(\frac{r_z^q}{\left|\vec{r}_k^q\right|}\right), \tag{5}$$

The orientation analysis can be translated into a simple condition where a point can be considered as non-traversable if $\alpha_q > \alpha_{max}$, where α_{max} is a user choice and it should be taken according to the vehicle capability. In Figure 3(b) a graphical explanation can be seen. The green vector r_1 can be considered to be ground, whereas the red vector r_2 belongs to a non-traversable surface. Their angles are respectively α_1 and α_2, and they are supposed to be $\alpha_1 < \alpha_{max} < \alpha_2$.

Figure 3 Orientation analysis applied on a 3D reconstruction obtained through a stereocamera images triangulation: (a) The orientation analysis superimposed on the camera image: the green arrow marks a typical normal vector belonging to the ground, whereas the red arrows mark typical normal vectors belonging to obstacles. In blue the vehicle reference frame; (b) Geometric interpretation of the orientation analysis based on the UPD

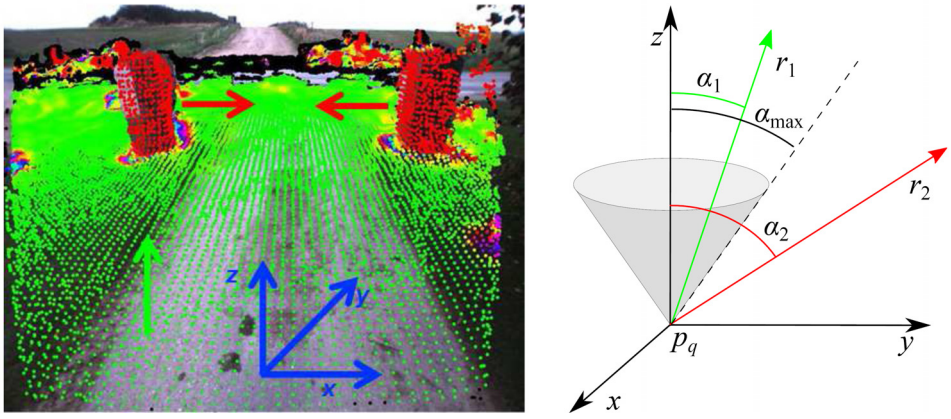

(a) (b)

3.2 UPD based path planning

The description of terrains, or with more generality scenes, is finalised to compute safe robots movements according to environmental information (Ojeda et al., 2006). The UPD fits really well for this task, since it takes into account the terrain roughness using visual information. To demonstrate this practical usefulness, the UPD has been applied in a path planning task.

The planner studied for this simulation is a stand-alone discrete planner on already processed 3D data in the form of a point cloud. Hence, only the planning primitive will be considered, assuming sensory information as already acquired, no movement constraints are applied and the robot is considered as a free-fly-point. First the discrete planning problem will be defined, then a point cloud, processed with UPD, will be used to obtain a cost map. At this aim, the UPD will be integrated into the cost function in order to compute optimal safe paths. Finally, the results of the planning on such cost map will be exposed.

Recent approaches in this field involve the study of discrete maps such as DEMs recently used in the path planning for mobile robot on rough terrain in volcano exploration (Ohki et al., 2013). In contrast to this approach that creates the digital map from 3D laser data and then computes a cost of each cell, the UPD based planner can directly work on 3D data avoiding loss of performance during the DEM generation.

Now, drawing on LaValle (2006), where the classical theory works of motion planning can be found, let us define discrete planning problem considering the following hypothesis:

1 Let $X \neq \varnothing$ be the space state;

2 $\forall x \in X$ let be defined the command space U;

3 Let be defined a transition function $f(x,u) \in X \quad \forall x \in X, u \in U$ and let be the transition function derivable as $\dot{x} = f(x,u)$;

4 Let $x_s \in X$ be the initial state, or start state, and $x_g \in X$ the goal state.

Under this hypothesis, the objective is finding a finite succession of k consecutive actions $\pi_k = \{u_1, u_2, \ldots u_k \in U\}$ such that $x_{i+1} = f(x_i, u_i) \forall i = 1,2,\ldots,k$, $x_0 = x_s$ and $x_k = x_g$.

This problem may have, in general, multiple solutions. From a robotic point of view, it is worth to ask which solution is the optimum and which factors affect the optimality of such solution.

Although in literature a large number of ways to solve such problem considering the shortest path according to a distance norm exist, the context of this work aims to find an optimal solution that considers also the roughness of the pavement. For this purpose, given a motion plan as the succession of k actions π_k, the cost function is given by the following relation:

$$L(\pi_k) = \sum_{i=1}^{k} (w_l l_i + w_t T_i), \tag{6}$$

where l_i is the *length of the step i* or rather the distance between two states calculated as the Euclidean distance, T_i is so-defined as *traversability index* that indicate the cost associated to the traversability of the state i, and w_l, w_t are weights associated to the length and the traversability, respectively.

Given a cost function, the problem moves to find the optimal motion plan π_k^* such that $L(\pi_k)$ is minimum, hence:

$$\min L(\pi_k) = L(\pi_k^*). \tag{7}$$

Now, it is possible to find the optimal path according to the factors in equation (6), i.e. length and traversability, and by the minimisation of equation (7).

For the proper application of UPD index in the minimisation of the cost function, let us better characterise the traversability index T_i. First, the traversability index expresses the traversabilty characteristics of a specific state, which, in this circumstance, is a point in the space. It must be remarked that, the context of this planner considers space information in the form of a point cloud. Hence, as a hypothesis for the practical implementation of this planner, each possible state is associated to one single point of the cloud and each single point has its associated UPD descriptor F_U, according to equation (3).

As a consequence, considering the cost function in equation (6), the traversability index in the query point p_q can be calculated as follows:

$$T_q = \begin{cases} \infty, & if \ \alpha_q \geq \alpha_{max} \\ \dfrac{1}{\zeta_k^q}, & if \ \alpha_q < \alpha_{max} \end{cases}, \tag{8}$$

where α_q has been defined in equation (5) as the orientation of the *r*-vector in specific query point, α_{max} is a user choice according to the vehicle capabilities and ζ_k^q is defined in equation (4) as the unevenness index associated to the point p_q. Regarding ζ_k^q, it is important to mention that it is an inverse index, since it is maximum in case of regular surfaces. For this reason has been used as inverse traversability index.

Note that the ratio $1/\zeta_k^q$ is always a positive real number other than zero since $\zeta_k^q > 0$ always. Indeed, ζ_k^q is positive-definite as the ratio between the norm of *r*-vector $\left|\vec{r}_k^q\right| \geq 0$ and the number of points $k > 0$ in the neighbourhood of p_q, see equation (4). It must be remarked that, the neighbourhood P_k^q must be not empty, it has to contain at least p_i, hence $k \geq 1$. The case of $k = 0 \Rightarrow P_k^q = \varnothing$ can be considered as trivial. As last remark, the *r*-vector derive from the sum of normal vectors those for convention always point upward, see Bellone et al. (2014a) where the ambiguity on the sign of the normal vectors has been explored. For this reason $\left|\vec{r}_k^q\right| \neq 0$ hence $\left|\vec{r}_k^q\right| > 0 \wedge k \geq 1 \Rightarrow \zeta_k^q > 0$. As a consequence also the traversability index T_q in the cost function can be considered as positive-definite.

4 Results

Experiments were performed in order to verify the effectiveness of the proposed approach for pavement distress detection. During the acquisition campaign, an experimental prototype car was driven on different types of roads, from regular urban road with new asphalt towards dirt roads presenting possible hazards. Images were acquired at 1 frame per second using a low-performance EeePC featuring an Intel Atom Processor. Although the frame rate may be increased using high performance computers, in this experiment the sampling rate can be considered reasonable considering typical travel speeds on irregular roads. In all figures the traversability map is shown on the left,

whereas the corresponding visual image is located on the right. Traversability maps have been calculated as the projection of the 3D cloud on the *xy*-plane. Hence, even though the UPD is calculated on a 3D cloud, the path planning refers to a 2D grid. In the traversability map green denotes traversable regions, whereas irregularities are denoted using increasing intensity colours. The optimal path is marked in black.

Road datasets are composed of thousands of images, however here we show relevant sample scenarios including: (i) a comparison between an elevation method and our UPD based computation; (ii) two typical road scenarios with both regular asphalt and pavement distress; and (iii) a night scenarios featuring a possible dangerous situation that can be properly handled by our system.

4.1 Comparison with existing methods

As a preliminary experiment, a comparison against an existing technique is considered. Common methods used in this field use the elevation above the ground to detect and recognise irregularities, however it is not always true that a change in elevation implies the presence of an irregularity. As an example, the scenario of Figure 4 shows a 20 degrees slope ramp to access an underground parking. The scene in Figure 4(c) is interpreted differently by the system that uses elevation information (traversability map of Figure 4(a)) than the one based on the UPD traversability map of Figure 4(b)). The green colour labels traversable cells, whereas uneven parts of the pavement are marked with increasing intensity colours.

Figure 4 Comparison between a standard and the UPD approach in the case of a ramp: the UPD method (b) properly recognises the region in the centre as not regular, whereas an elevation-based method (a) detects the slope as not regular surface: (a) Traversability map processed using the elevation, the intensity of the colour increases as the elevation of the patch; (b) Traversability map calculated using the UPD method, the intensity of the colour increase as the unevenness index decreases; (c) Corresponding camera image

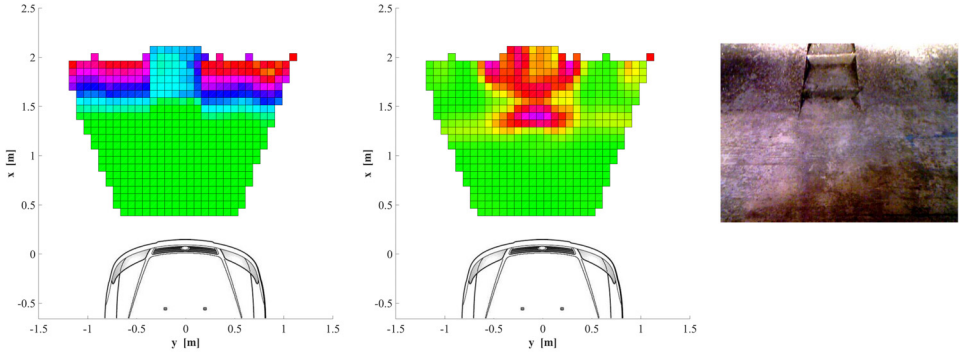

(a) (b) (c)

Owing to the change in elevation, the conventional approach fails to recognise the cells pertaining to the ramp as drivable. In contrast the UPD-based method correctly detects the central portion of the ramp as irregular due to the presence of the stairs, whereas the

sides are properly recognised as regular and traversable. In Figure 4(b) the intensity of the colour increases as the terrain irregularity, i.e. as the value of ζ_k^q decreases. As an additional detail, we can note that the use of the elevation method requires that 3D clouds must be represented into the vehicle reference frame and must be accurately calibrated, whereas an accurate calibration of the transformation in the case of UPD is not mandatory. This results in a reduction of possible misinterpretation using the UPD analysis. An additional advantage resides in a minor influence of the vehicle tilt on the global traversability performances, i.e. images do not require stabilisation using IMU roll and pitch estimates.

4.2 Analysis on road datasets

Although during the experimental campaign a large number of frames were acquired, here only significant scenarios are described. The first presented scenario in Figure 5 shows a smooth pavement where the UPD correctly detects the road as safe with a corresponding optimal path that does not deviate from a straight line. In this case the value of the unevenness index is always close to 1, the green colour has been used to denote regular surfaces. The corresponding visual image is reported on the right. Then, during the acquisition campaign, the vehicle was driven towards challenging roads. The frame presented in Figure 6 presents a dirt road with irregularities i.e. a strong pavement distress. Note that it is properly recognised by the UPD analysis, the increasing intensity in the colour of each patch in the traversability map marks the position of the pothole respect to the vehicle. Finally, the solver can automatically generate a path to avoid the pavement distress, labelled by colouring the corresponding cells as black. The regions that may be unsafe for the vehicle are labelled in Figure 6 by increasing intensity colours according to the unevenness index value.

Figure 5 Traversability map and generated path relative to a scenario featuring regular asphalt, the corresponding camera image is reported on the right, the generated path is marked using the black colour

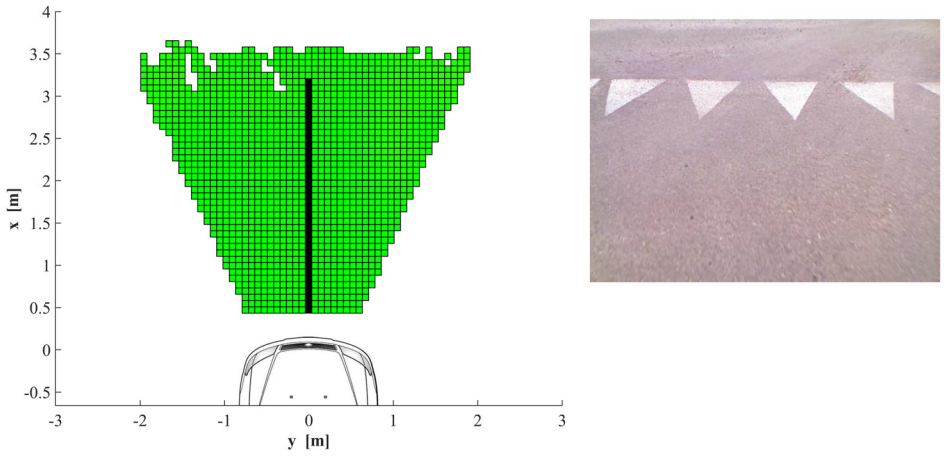

Figure 6 In the case of a strong pavement distress the traversability map features a wide hardly traversable region and the corresponding generated path deviates from a pure straight line to avoid the irregularity

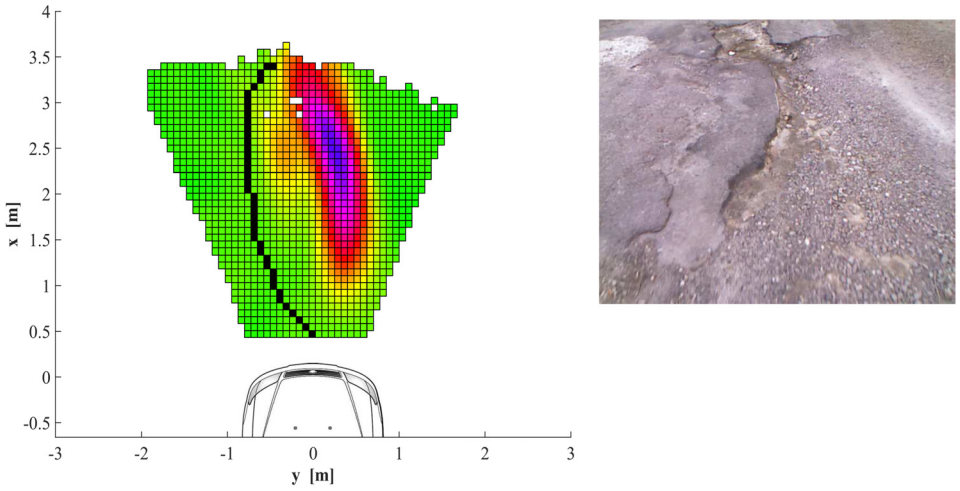

In order to better quantify this result, the histogram in Figure 7 is proposed; the distribution of the unevenness index for the two cases of regular (marked in green) and uneven (denoted by red) road are shown. The values compared in the histogram correspond to previously proposed scenarios with specific reference to Figures 5 and 6. As a histogram aims at categorising elements, the bin number represents the number of points in the cloud having the same unevenness value. It is evident that, for the first scenario the unevenness index is close to 1 and all points fall in the first bin, on the contrary, scenario 2 presents an irregularity and the bins are spread along the *x*-axis.

Figure 7 Histogram analysis showing a comparison between a regular surface (see Figure 5) and a pavement distress (Figure 6)

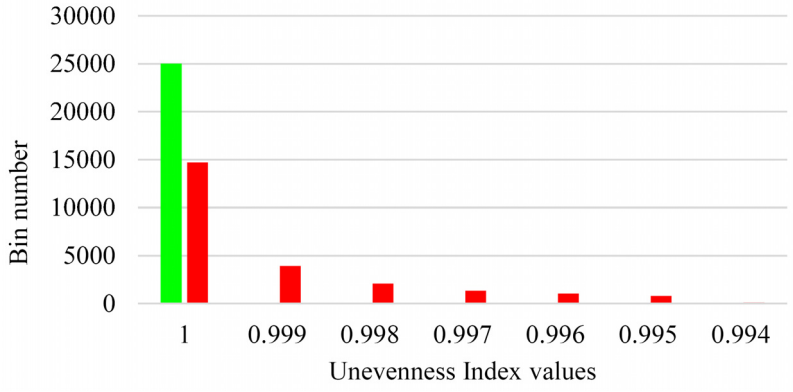

Notwithstanding that Kinect represents a good trade-off between performance and cost, it should be pointed out that such sensor has known limitation under direct sunlight. This issue greatly reduces the practical applicability of the Kinect in outdoor environments. Conversely, it works well under low lighting conditions, where the driver has reduced or compromised visibility. This is demonstrated in Figure 8, where a road hazard, (i.e. a pothole) in front of the car, is correctly detected by the system using the depth camera, whereas visual image is unusable in this case. This leaves space to the application of the same point descriptor to other high-end 3D sensor data. In general, point cloud processing with normal analysis can be successfully applied to road surface estimation, moreover the planner is able to properly drive the vehicle towards a safe region of the carriageway.

Figure 8 Under low-lighting conditions, a pothole can be hardly detected. Nevertheless, the proposed system was able to detect the hazard and plan a safe path for the vehicle

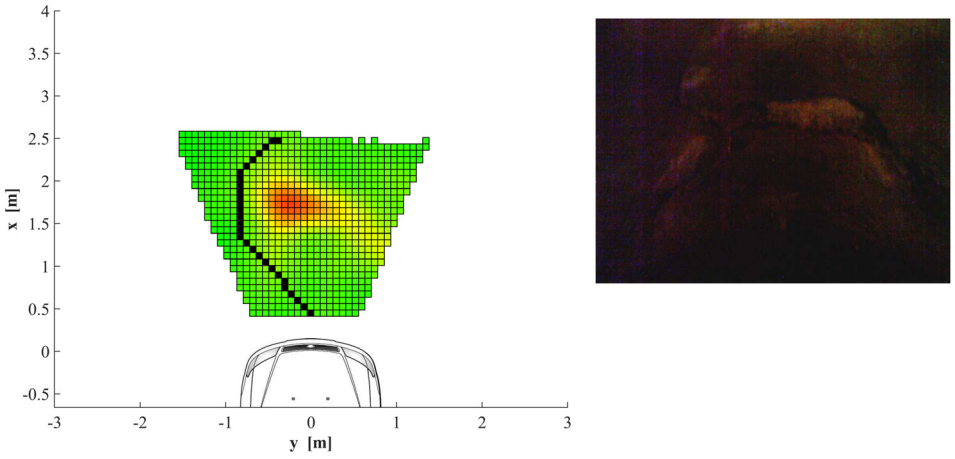

5 Conclusions

In this work, an extension of the use of the Unevenness Point Descriptor to pavement distress detection and avoidance has been proposed. The results show that the evolution of pavement distress detection is promising and may help to drastically reduce fatal traffic casualties, as a high percentage of road accidents is related to road irregularities. The depth camera used in this implementation is an off-the-shelf cost effective sensor, thus it could be easily integrated with commercial cars. This research has been conducted including an acquisition campaign and a post analysis of grabbed data. The results encourage future research since it was demonstrated that the UPD-based method for pavement distress detection and avoidance can: (i) generate safe and free-collision paths in case of irregular pavement; (ii) directly work on a 3D based space reconstruction avoiding digital elevation maps processing; and (iii) let the planner generate feasible paths thanks to the pre-sizing of a size parameter for the calculation of the UPD even

though no robot geometric shape has been considered. As a further improvement, it would be possible to implement a reactive technique which might consider the irregularity for a proper navigation also considering kinematic or dynamic constraints of the robot.

References

Bellone, M., Messina, A. and Reina, G. (2013a) 'A new approach for terrain analysis in mobile robot applications', *IEEE International Conference on Mechatronics (ICM) 2013*, pp.225–230.

Bellone, M., Pascali, L. and Reina, G. (2014a) 'A kinect-based parking assistance system', *Advances in Robotics Research, An International Journal*, Vol. 1, No. 2, pp.127–140.

Bellone, M., Reina, G., Giannoccaro, N.I. and Spedicato, L. (2013b) 'Unevenness point descriptor for terrain analysis in mobile robot applications', *International Journal of Advanced Robotic Systems*, Vol. 10, p.284.

Bellone, M., Reina, G., Giannoccaro, N.I. and Spedicato, L. (2014b) '3D traversability awareness for rough terrain mobile robots', *Sensor Review*, Vol. 34, No. 2, pp.220–232.

Broggi, A., Cardarelli, E., Cattani, S. and Sabbatelli, M. (2013) 'Terrain mapping for off-road autonomous ground vehicles using rational b-spline surfaces and stereo vision', *2013 IEEE International Conference on Intelligent Vehicles Symposium (IV)*, June, pp.648–653.

Holz, D., Holzer, S., Rusu, R.B. and Behnke, S. (2011) 'Real-time plane segmentation using RGB-D cameras', *Proceedings of the 15th RoboCup International Symposium*, DOI 10.1007/978-3-642-32060-626.

Holzer, S., Rusu, R.B., Dixon, M., Gedikli, S. and Navab, N. (2012) 'Adaptive neighborhood selection for real-time surface normal estimation from organized point cloud data using integral images', *International Conference on Intelligent Robots and Systems (IROS), 2012 IEEE/RSJ*, October, pp.2684–2689.

Howard, A. and Saraji, H. (2001) 'Vision-based terrain characterization and traversability assessment', *Journal of Robotic Systems*, Vol. 18, No. 10, pp.77–587.

ISTAT (2013) *Rapporto Anno 2012 – Incidenti stradali in Italia*, November.

Kim, T. and Ryu, S. (2014) 'Review and analysis of pothole detection methods', *Journal of Emerging Trends in Computing and Information Sciences*, Vol. 5, No. 8, pp.603–608.

LaValle, S.M. (2006) *Planning Algorithms*, Cambridge University Press.

Mphahlehle, J., Joubert, D., Tyatyantsi, A. and Manchidi, V. (2011) 'Pothole tagging system', *Proceedings of the 4th Robotics and Mechatronics Conference of South Africa*.

Nam, B., Lee, J. and Abdel-Aty, M. (2015) 'Effects of pavement surface conditions on traffic crash severity', *Journal of Transportation Engineering*, DOI: 10.1061/(ASCE)TE.1943-5436.0000 785.

Ohki, T., Nagatani, K. and Yoshida, K. (2013) 'Path planning for mobile robot on rough terrain based on sparse transition cost propagation in extended elevation maps', *IEEE International Conference on Mechatronics and Automation (ICMA)*, August, pp.494–499.

Ojeda, L., Reina, G., Cruz, D. and Borenstein, J. (2006) 'The FLEXnav precision dead-reckoning system', *International Journal of Vehicle Autonomous Systems*, Vol. 4, No. 2, pp.173–195.

Oniga, F. and Nedevschi, S. (2010) 'Processing dense stereo data using elevation maps: road surface, traffic isle, and obstacle detection', *IEEE Transactions on Vehicular Technology*, Vol. 59, No. 3, pp.1172–1182.

Osari, H. (2003) 'A new method for assessing land leveling to produce high quality consolidated paddy fields', *Paddy and Water Environment*, Vol. 1, No. 1, pp.35–41.

Rohmer, E., Reina, G. and Yoshida, K. (2010) 'Dynamic simulation-based action planner for a reconfigurable hybrid leg-wheel planetary exploration rover', *Advanced Robotics*, Vol. 24, Nos. 8/9, pp.1219–1238.

Rusu, R.B. (2009) *Semantic 3D Object Maps for Everyday Manipulation in Human Living Environments*, Munich, Germany.

Rusu, R.B. and Cousins, S. (2011) '3D is here: point cloud library (pcl)', *IEEE International Conference on Robotics and Automation (ICRA)*, Shanghai, China.

Rusu, R.B., Marton, Z.C., Blodow, N. and Beetz, M. (2008) 'Learning informative point classes for the acquisition of object model maps', *10th International Conference on Control, Automation, Robotics and Vision*, Hanoi, Vietnam.

Seraji, H. (1999) 'Traversability index: a new concept for planetary rovers', *IEEE International Conference on Robotics and Automation*, Detroit, MI, USA, pp.2006–2013.